Korean J. Chem. Eng., 36(6), 965-974 (2019)
DOI: 10.1007/s11814-018-0230-1

pISSN: 0256-1115
eISSN: 1975-7220

Synergistic decomposition of imidacloprid by TiO_2-Fe_3O_4 nanocomposite conjugated with persulfate in a photovoltaic-powered UV-LED photoreactor

Mohammad Reza Eskandarian*,,***, Mohammad Hossein Rasoulifard**,†,‡, Mostafa Fazli*, Leila Ghalamchi**, and Hyeok Choi***,†,‡**

*Department of Applied Chemistry, Faculty of Chemistry, Semnan University, Semnan 363-35196, Iran
**Water & Wastewater Treatment Research Laboratory, Department of Chemistry, University of Zanjan, Zanjan 313-45195, Iran
***Department of Civil Engineering, The University of Texas at Arlington, Arlington, TX 76019-0308, United States
(*Received 9 October 2018 • accepted 17 January 2019*)

Abstract−To facilitate decomposition of imidacloprid (IMD), as a persistent probe insecticide, TiO_2-Fe_3O_4 (TF) nanocomposite was synthesized and characterized. TF particles in size of 50-60 nm with band-gap of 2.8 eV were immobilized onto glass tubes and utilized as a photocatalyst irradiated with ultraviolet-light emitting diode (UV-LED) powered by photovoltaics. Synergistic decomposition of IMD in the photocatalytic reactor injected with persulfate (PS) was investigated. Along with various control and reference tests, parametric studies to evaluate the effects of PS concentration, IMD concentration, and circulation rate on IMD decomposition kinetics and electrical energy consumption were performed. The contribution of various physical and chemical mechanisms to IMD removal was discussed, including self-decomposition, direct photolytic decomposition, chemical oxidation by PS, photolysis of PS to produce sulfate radicals, Fenton-like reaction to produce sulfate radicals, photocatalysis to generate hydroxyl radicals, and adsorption onto catalysts. TF conjugated with PS under UV-LED synergistically decomposed IMD. Additionally, results demonstrated the synergy index factor of 75%, 65%, and 60% for IMD degradation by UV-LED/TF/PS, UV-LED/Fe_3O_4/PS, and UV-LED/TiO_2/PS routes, respectively. Outcomes also showed that utilizing TF can greatly reduce electrical energy consumption. Since all devices used in this study, including UV-LED, were powered solely by a photovoltaic module, the immobilized TF photoreactor was proposed as a sustainable, self-powered, energy-saving, and practical point-of-use decontamination system to remove organic contaminants in water under solar radiation.

Keywords: Imidacloprid, Persulfate, Photocatalysis, Photovoltaics, TiO_2-Fe_3O_4, UV-LED

INTRODUCTION

Around 1-2.5 million tons of active pesticide ingredients are used annually, mainly in agriculture [1-6]. Based on the report by the United States Environmental Protection Agency, imidacloprid (IMD) is considered a highly toxic insecticide [7]. IMD is made to mimic nicotine and it acts as an insect neurotoxin. Leaching of IMD often causes groundwater contamination because of its high solubility and mobility. Among many treatment processes to decompose such persistent and non-biodegradable contaminants in water, advanced oxidation processes (AOPs) have recently gained significant attention [8-10]. Highly oxidizing transient radical species such as hydroxyl radicals are generated in AOPs and readily and non-selectively attack organic chemicals [10-13]. As one of the most promising AOPs, photocatalysis using titanium dioxide (TiO_2) is significant due to its effectiveness in generating radicals under ultraviolet (UV) radiation and many other advantages such as low cost and chemical stability [14-17]. In addition, many investigations have been conducted with TiO_2 as photocatalyst because of its unique features for water splitting, hydrogen evolution, and other environmental remediation approaches [18,19]. AOPs also include UV-based chemical oxidation processes such as O_3/UV, H_2O_2/UV, and O_3/H_2O_2/UV, and their combination with TiO_2 photocatalysis such as H_2O_2/UV/TiO_2 [20-27].

In those AOPs, O_3 and H_2O_2 have been commonly used as oxidants to produce mostly robust hydroxyl radicals (E_0=2.8 eV) [28-32]. In recent years, there has been also huge research effort to introduce persulfate (PS) to substitute O_3 and H_2O_2 in the AOPs [31,32]. PS is a more cheap, stable, and safe oxidant than others, and is decomposed under UV radiation to produce sulfate radicals (E_0=2.6 eV) [33,34]. Sulfate radicals are as strong as hydroxyl radicals and they are relatively more selective than hydroxyl radicals. Sulfate radicals might work in a wide range of pH conditions. They are known to be more reactive for some organic chemical groups than hydroxyl radicals [33,34].

Consequently, the combination of PS/UV system with TiO_2 photocatalysis might have high potential to synergistically decompose persistent organic contaminants such as IMD. In this present study for decomposition of IMD by PS/UV/TiO_2, two important technical aspects were addressed. First, TiO_2-Fe_3O_4 (TF) nanocomposite was examined instead of pure TiO_2 [35-38]. Due to the magnetic property of Fe_3O_4, TF composite can be easily removed by applying a magnetic field after its applications for water treatment [39-

†To whom correspondence should be addressed.
E-mail: m_h_rasoulifard@znu.ac.ir, hchoi@uta.edu
‡The two authors contributed equally to this work.

43]. According to the energy level theory, the presence of Fe_3O_4 can also enhance the photocatalytic activity of TiO_2 [44-46]. Eventually, TF composite will be immobilized onto glass tubes to build a more sustainable and practical photocatalytic reactor composed of PS/UV/TF.

Second, light emitting diodes (LEDs) instead of mercury-based UV lamps were used to activate PS and TF, so-called UV-LEDs [47-50]. Recently, UV-LEDs have been widely introduced as greener light sources in various photochemical and photocatalytic processes for degradation of water contaminants. UV-LEDs show many advantages such as better energy efficiency, longer lifetime, no warm-up time, and no mercury disposal problem [50,51]. In particular, UV-LEDs exhibit higher quantum yields [51,52]. In this study, UV-LEDs were also be powered by photovoltaics (PV). Considering that most of the developing countries have limited energy sources and demand point-of-use applications, such a PV-based photochemical and photocatalytic process might be essential for in-situ small-scale water treatment and disinfection [53-63].

As a result, the overall objective of this study was to evaluate the synergistic decomposition of IMD by immobilized TF nanocomposite conjugated with PS in a PV-powered UV-LED photoreactor. Physical and chemical mechanisms for the removal of IMD were elucidated, including self-decomposition, direct photolytic decomposition, chemical oxidation by PS, photolysis of PS to produce sulfate radicals, Fenton-like reaction to produce sulfate radicals, photocatalysis to generate hydroxyl radicals, and adsorption onto catalysts. Along with various control and reference tests, parametric studies to evaluate the effects of PS concentration, IMD concentration, and circulation rate on IMD decomposition kinetics and electrical energy consumption were performed. The TF photoreactor is proposed as a sustainable, self-powered, energy-saving, and practical point-of-use decontamination system to remove organic contaminants in water under solar radiation.

EXPERIMENTAL

1. Chemicals and Materials

IMD was purchased from Aria Shimi Co. (Iran) and used as received. The chemical properties of IMD are reported in Table S1. Potassium persulfate ($K_2S_2O_8$), sodium hydroxide (NaOH), and hydrofluoric acid (HF) were purchased from Merck (Germany). Ethanol (C_2H_5OH) was purchased from Zakariya Razi Co. (Iran). Double distilled water was utilized for all experiments (GFL, type 2008, Germany). TiO_2 nanoparticles (Degussa P-25) with surface area of 55 m^2/g and in size of 30 nm were supplied by Fluka (Germany). Ferrous chloride ($FeCl_2{\cdot}6H_2O$) and ferric chloride ($FeCl_3{\cdot}6H_2O$) (Merck, Germany) were used for synthesis of Fe_3O_4 nanoparticles. Glass tubes used as a substrate for catalyst immobilization were obtained from a local glass company (Zanjan, Iran).

2. Synthesis of Magnetic TiO_2-Fe_3O_4 Nanocomposite Immobilized onto Glass Tubes

To synthesize Fe_3O_4 nanoparticles, 50 mL of 1 mol/L $FeCl_3{\cdot}6H_2O$ and 50 mL of 2 mol/L $FeCl_2{\cdot}6H_2O$ were poured into 100 ml beaker and sonicated in a bath sonicator at 100 W for 20 min. Then, 25 mL of 1 mol/L NaOH was added into Fe solution, forming black iron oxide precipitates. To complete the precipitation process, the solution was continuously sonicated at 60 °C for 30 min. Then, only magnetic Fe_3O_4 particles were separated by applying a magnetic field with 1.2 T field strength supermagnet (Kanetec, Japan) [39-41].

To prepare TF nanocomposite particles, i.e., TiO_2-Fe_3O_4, equal amounts of TiO_2 nanoparticles and Fe_3O_4 nanoparticles were added into C_2H_5OH to achieve total solid concentration of 33 g/L and the suspension was sonicated to segregate particles at 100 W and 60 °C for 40 min. Before particle immobilization, the outer surface of glass tubes with length of 150 mm and diameter of 15 mm was scratched with carbide tungsten grinding stone (Shimi Azma, Iran) and washed with diluted HF followed by NaOH solutions. TF suspension was carefully poured and uniformly descended down onto glass tubes. After drying to remove C_2H_5OH at room temperature, TF-immobilized tubes were calcined in a furnace at 480 °C for 3 hr to enhance mechanical adherence strength. Then, they were finally washed with water several times to remove un-integrated TiO_2 and Fe_3O_4 particles. This cycle was repeated three times to ensure enough TF particles were immobilized onto glass tubes. As references, only TiO_2 particles and only Fe_3O_4 particles were also immobilized onto glass tubes by following the exact same procedure above for TF.

3. Characterization of TiO_2/Fe_3O_4/TF Catalysts

The amounts of the catalysts loaded onto glass tubes were determined by monitoring weight change before and after coating. Visual morphology of the catalysts was investigated with field emission scanning electron microscopy (SEM/TESCAN MIRA3-FEG, United States). Surface functional groups were analyzed with Fourier transform infrared spectroscopy (FT-IR, iS 10Thermo Nicolet, England). X-ray diffraction (XRD) pattern was collected with XRD instrument (XRD-D8 ADVANCED-BRUCHERS AXS, Germany) to investigate the crystallographic properties. Energy dispersive X-ray (EDX) spectroscopy connected to SEM was used to conduct elemental analysis and eventually elemental mapping. To find the synergistic effect of co-catalyst Fe_3O_4 on the photocatalytic activity of TiO_2, the band-gaps of TF and TiO_2 were measured by UV-visible diffuse reflectance spectra (DRS) analysis (Cary 500, Varian Co., Agilent Technologies, Australia) [39-44].

4. UV-LED Reactor Setup and IMD Decomposition

The UV-LED photoreactor used in this study is shown in Fig. 1 (also note Fig. S1). The reactor had two chambers with internal circulation; one with UV-LED (the first chamber in the figure) and the other with UV-LED and catalysts (the second chamber). The first chamber with diameter of 15 cm and height of 28 cm had effective volume of 5,000 mL while the second chamber with diameter of 15 cm and height of 14 cm had effective volume of 2,500 mL. The chambers had double-walls. Six glass tubes loaded with total around 1,875 mg of catalysts (TiO_2, Fe_3O_4, or T-F) were installed between the walls of only the second chamber. Inside of both chambers, 66 UV-LED lamps with 1 W power each (Optodevice, South Korea) irradiated UVA at λ_{max}=390 nm measured by ultrafast fiber optic spectrometer (AvaSpec-128, Avantes, Netherlands). PV module with power range of 225-250 W and efficiency range of 13.8-15.3% (TN-P225-250, Energy Technology, China) was used to harvest electrical power from solar radiation and thus to operate all devices used in this study, including UV-LEDs and pumps. IMD

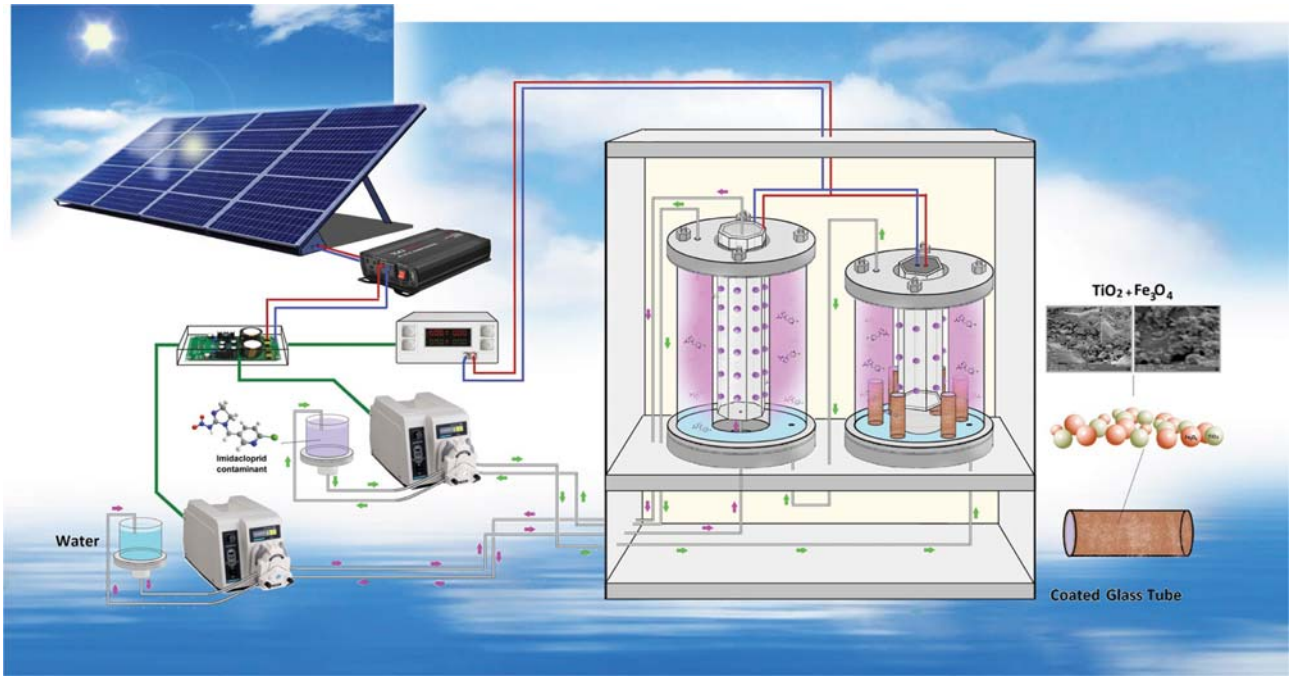

Fig. 1. Photovoltaic-powered UV-LED photoreactor with two chambers: first one with UV-LED and second one with UV-LED and catalysts. The reactor *setup*was considered as batch with internal circulation. The reactor setup made it possible to conduct various types of photolytic, photocatalytic, oxidative, and enzymatic experiments in the reactor not only for this study but also for many other studies. All devices used in this study were powered by a photovoltaic module.

solution was first provided to the second chamber for photocatalysis and then the effluent continuously passed through the first chamber for UV-LED irradiation. Finally, the effluent was recirculated within the whole system. The reactor setup is more or less complex, but such a setup makes it possible to conduct various types of photolytic, photocatalytic, oxidative, and enzymatic experiments in the reactor not only for this study but also for many other studies.

The reactor setup is considered as batch with internal circulation at 100 mL/min. All reactions proceeded for 4 hr in the batch reactor, and thus overall hydraulic residence time (HRT) was also 4 hr. Considering that the amount of solution in the tubes, pumps, and auxiliary containers was negligible, the first and second chambers had 160 min and 80 min of HRT, respectively. Standard operational conditions were 250 mg/L of catalyst, 20 mg/L of IMD, 20 mM of PS, 100 mL/min of circulation rate, 66 W of UV-LEDs, and 25 °C of temperature. For parametric studies, IMD concentration at 10-40 mg/L, PS concentration at 0-120 mM, and circulation rate at 100-375 mL/min were varied. Note that changing the circulation rate did not affect HRT in each chamber. All experiments were performed without controlling pH and using buffer. Initial pH at around 6 decreased slightly over reaction. A UV-Visible spectrophotometer (DR 5000, Hach, USA) was employed to measure IMD concentration. UV absorption intensity at λ_{max}=270 nm was correlated with IMD concentration as demonstrated elsewhere [64].

RESULTS AND DISCUSSIONS

1. Properties of TiO_2, Fe_3O_4, and TF

The properties of TiO_2, Fe_3O_4, and TF were briefly characterized.

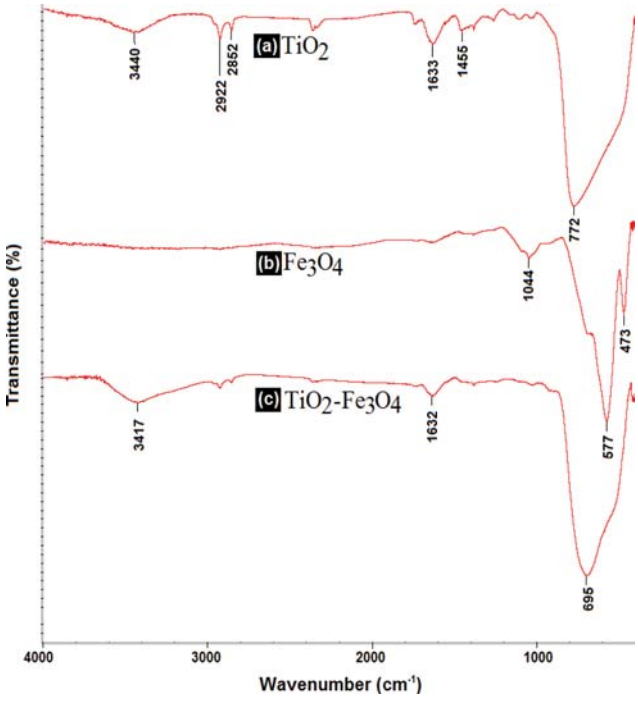

Fig. 2. FT-IR spectra for (a) TiO_2, (b) Fe_3O_4, and (c) TF composite.

The results are important to explain the observed reactivity of various systems later. FT-IR analysis of TF is shown in Fig. 2. The absorption peaks represented the presence of TiO_2 and Fe_3O_4 and shift of some peaks and formation of new peaks were also observed.

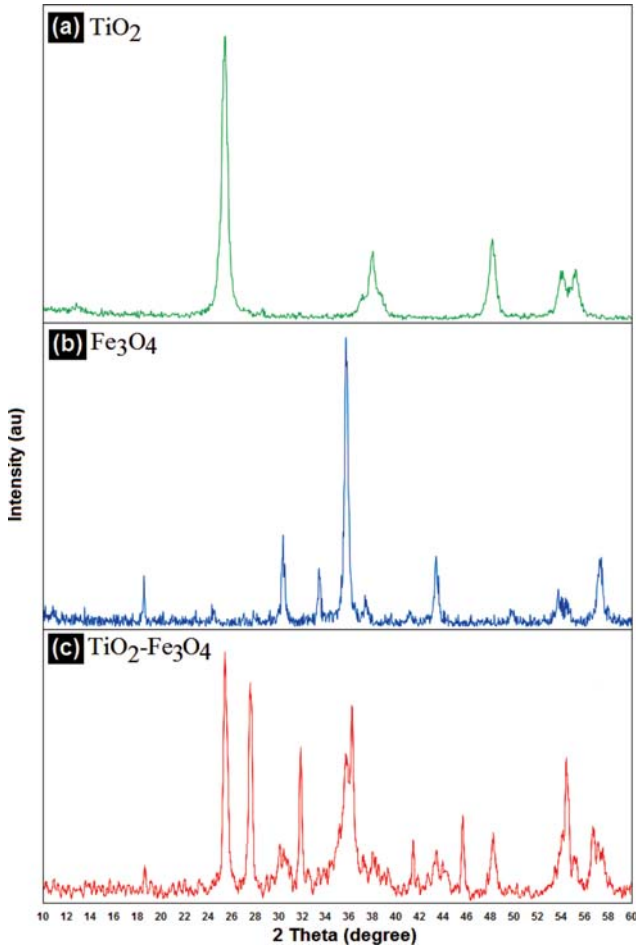

Fig. 3. XRD pattern for TiO_2, Fe_3O_4, and of TF composite.

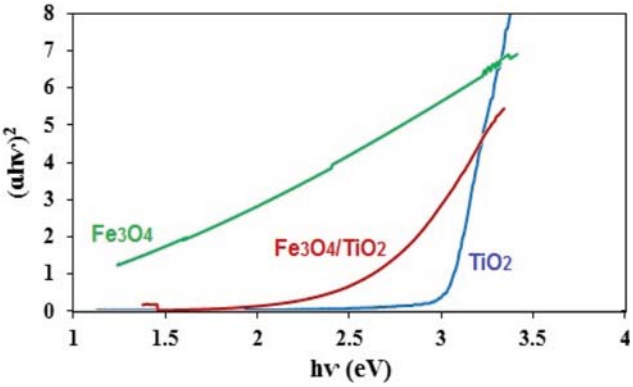

Fig. 4. Band-gap analysis for TiO_2, Fe_3O_4, and of TF composite.

OH bending vibration band for TF appeared at 3,430 cm^{-1}, which is close to that for TiO_2 typically at 3,440 cm^{-1} but far from that for Fe_3O_4 at 3,413 cm^{-1}, suggesting that Fe_3O_4 was somehow surrounded by TiO_2. The observation was further supported by the disappearance of a peak at 580 cm^{-1}, which corresponds to Fe-O stretching vibration in Fe_3O_4 [40]. Fe-O vibration absorption band presumably in Ti-O-Fe bridge structure was observed at 497 cm^{-1}, indicating substitution of Ti in Ti-O-Ti lattice with Fe [40-42]. The result indicated formation of new TF nanocomposite, rather than heterogeneous mixture of TiO_2 and Fe_3O_4. Fig. 3 shows XRD pattern of TF. All peaks well indicated the crystal structures of TiO_2 and Fe_3O_4 [65-67]. Based on the Scherrer equation, the crystal sizes of TiO_2 and Fe_3O_4 were at around 30 nm and 23 nm, respectively [67]. Fig. 4 shows DRS analysis result to determine the band-gaps of TiO_2 and TF. TiO_2 showed band-gap at around 3.17 eV. Since this study used P-25, 7 : 3 mixture of anatase (3.2 eV) and rutile (3.0 eV), the band-gap at 3.17 eV was well expected. Also, in the present study a 1 : 1 loading ratio for TiO_2 : Fe_3O_4 in TF nanocomposite was considered. Meanwhile, TF showed much reduced band-gap at 2.78 eV. Adding co-catalyst Fe_3O_4 to TiO_2 was beneficial to reduction of the band-gap of TiO_2 in addition to magnetic removal of TiO_2 [44-46]. The reduced band-gap of TF might lead to better reactivity in UV-LED photocatalytic systems [40-45].

Fig. 5 shows SEM images of Fe_3O_4, TiO_2, and TF supported onto glass tubes. Formation of Fe_3O_4 nanoparticles is clear in Fig. 5(a). Fe_3O_4 nanoparticles are uniformly dispersed onto glass substrate. The similar result was also observed for TiO_2 in Fig. 5(b). TiO_2 particles were slightly larger than Fe_3O_4, which agrees with the crystal sizes of the particles (30 nm and 23 nm). TF exhibited aggregated mixture of TiO_2 and Fe_3O_4. TF composite was still at nanoscale much less than 100 nm. All the results proved uniformly dispersed and stably immobilized nanoscale catalysts. EDX result shown in Fig. S2 supports the presence of Ti and Fe in TF composite. Ti and Fe content was 23.2% and 10.3% (as weight), respectively. Elemental mapping of TF composite shown in Fig. S3 also indicates that Ti and Fe elements were uniformly distributed. Ti was more fre-

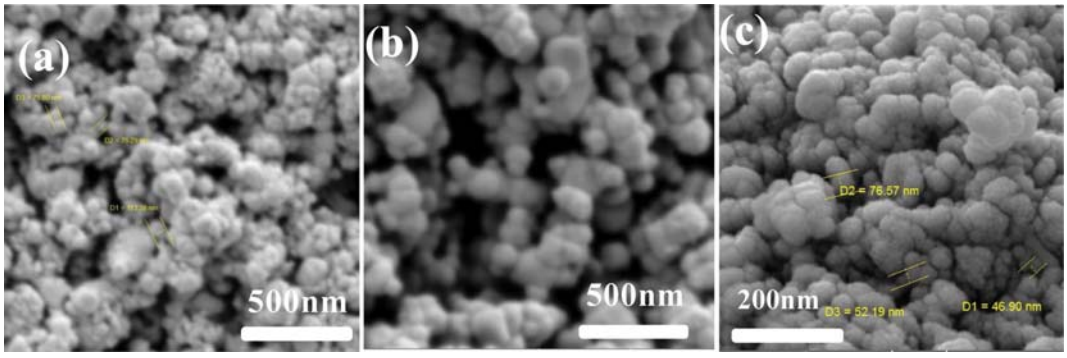

Fig. 5. SEM images (a) Fe_3O_4, (b) TiO_2, and (c) TF composite. TF image was obtaniend at higher magnification to distinguish Fe_3O_4 and TiO_2.

quently mapped than Fe, supporting the previous observation that Fe_3O_4 was somehow covered by TiO_2.

2. Comparative Reactivity of Various Combinational Systems

Various photochemical and photocatalytic processes of UV-LED, catalysts, and PS alone and in combination were performed as controls and references. As summarized in Table 1, several decomposition mechanisms, including self-decomposition (R1), direct photolytic decomposition (R2), chemical oxidation by PS (R3), photolysis of PS to produce sulfate radicals (R4), Fenton-like reaction to produce sulfate radicals (R5), and photocatalysis to generate hydroxyl radicals (R6) were considered to explain the removal of IMD in each process. The removal was also partly ascribed to adsorption of IMD onto catalysts (A1). Note that when IMD decomposition occurred in this photoreactor, its concentration kept decreasing in some cases, implying that the reaction did not reach steady-state.

2-1. Single Component

Results on single component are shown in Fig. 6(a). IMD itself (indicated as control) was stable and thus not decomposed, i.e., no R1 mechanism. There was also negligible photolytic decomposition of IMD under UV-LED, i.e., no R2 mechanism. The absence

Table 1. Possible removal mechanisms for IMD

Index	Mechanism	Required conditions
R1[a]	Self-decomposition	None
R2[a]	Direct photolytic decomposition	UV-LED
R3	Chemical oxidation by PS	PS
R4	Photolysis of PS to produce sulfate radicals	UV-LED and PS
R5[b]	Fenton-like reaction to produce sulfate radicals	PS and catalysts[c]
R6	Photocatalysis to generate hydroxyl radicals	UV-LED and catalysts
A1	Adsorption onto catalysts	Catalysts

[a]R1 and R2 were negligible under given conditions and thus their contributions to IMD removal were not taken into consideration later
[b]Fenton-like reaction is likely to occur when catalysts contain small amounts of transition metals such as Fe
[c]TiO_2, Fe_3O_4, and TF

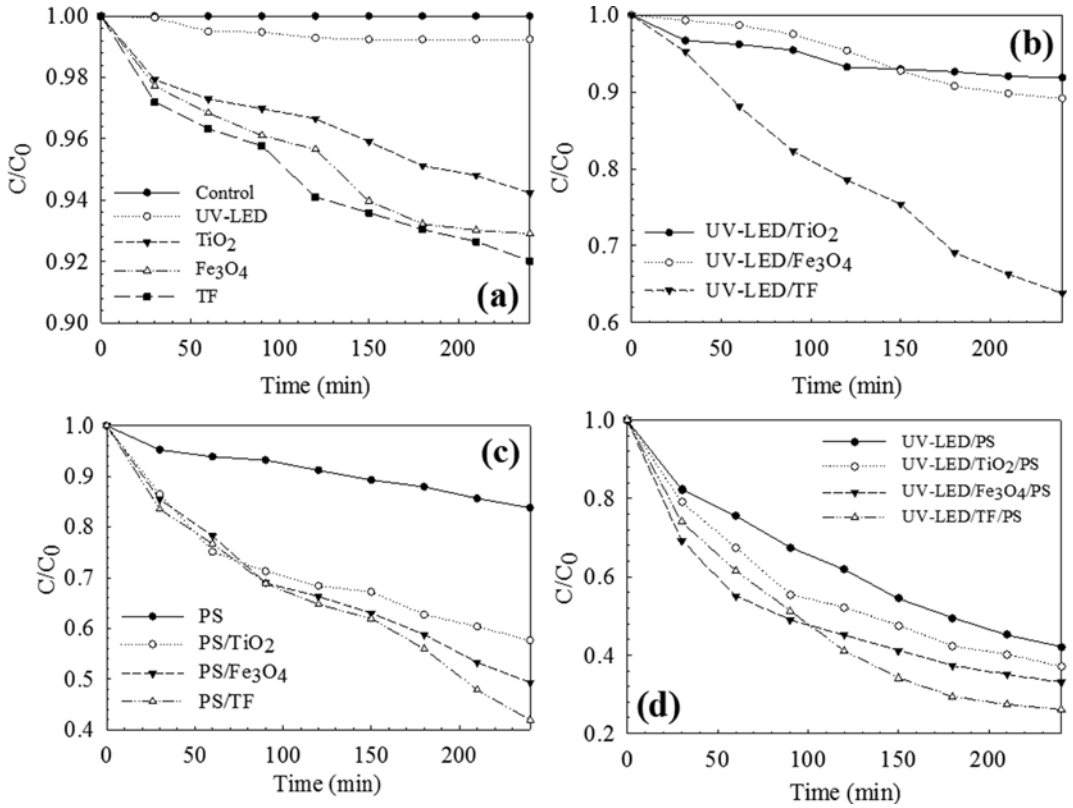

Fig. 6. IMD degradation in various control and reference tests: (a) Single control, (b) UV-LED/catalyst, (c) PS/catalyst, and (d) UV-LED/PS/catalyst (UV-LED=66 W, I=1.40 A, $pH_{initial}$~6, T=25 °C, [TF]=250 mg/L, [IMD]=20 mg/L, [PS]=120 mM, and circulation rate=100 mL/min). Please note that different Y axis scales were used in each figure to visualize differences in IMD degradation kinetics. Also, in order to quickly compare the reactivity of various combinational systems, the highest concentration of PS at 120 mM was used in this test, not 20 mM which is standard condition.

of R1 and R2 mechanisms makes it easy to quantify the contributions of other removal mechanisms. R1 and R2 mechanisms were not taken into consideration later. TiO_2, Fe_3O_4, and TF alone (A1 mechanism) removed at most around 6%, 7%, and 8%, respectively, due to adsorption of IMD. Moreover, Zeta potential analysis was conducted for better understanding of the adsorption mechanism. BET Analysis illustrated values as follows: (Fe_3O_4=58.98 m^2g^{-1}), (TiO_2=50 m^2g^{-1}) and (TF=62.7 m^2g^{-1}).

2-2. UV-LED/Catalysts

Photocatalytic decomposition of IMD by TiO_2, Fe_3O_4, and TF under UV-LED is shown in Fig. 6(b). All experiments were conducted based on IMD UV-Vis spectra (Fig. S4). Since R1 and R2 are negligible, any removal of IMD can be explained by R6 and A1. TiO_2/UV-LED and Fe_3O_4/UV-LED exhibited IMD removal at 8% and 10%, respectively. Considering the magnitude of A1 in the previous case, the contribution of photocatalysis to IMD removal, R6, was very low at less than 2-3%. TiO_2/UV-LED and Fe_3O_4/UV-LED under the given condition seemed to be ineffective to generate hydroxyl radicals for the decomposition of IMD. This is because UV-LED used in this study with λ_{max}=390 nm did not effectively activate TiO_2 with band-gap of 3.17 eV. In general, most TiO_2 photocatalysts require UV at λ_{max}=365 nm. Meanwhile, TF/UV-LED was able to significantly remove IMD via photocatalytic decomposition mechanism, R6. The high reactivity of TF can be ascribed to its narrow band-gap at 2.78 eV corresponding to 445 nm. UV-LED at λ_{max}=390 was effective enough to activate TF. Other unique properties of TF mentioned previously might have impacted the reactivity [68].

2-3. PS/Catalysts

Reaction between PS and catalysts was evaluated to remove IMD via R3, R5, and A1 mechanisms, as shown in Fig. 6(c). IMD was recalcitrant enough to resist chemical decomposition by PS alone as a strong oxidant. Only 16% of IMD was decomposed by PS (R3). There was significant decomposition of IMD when PS was coupled with TiO_2<Fe_3O_4<TF due to mainly additional R5 mechanism and partly A1 mechanism. The reason for the increased reactivity of PS/Fe_3O_4 and PS/TF seems to be obvious. It is known that PS can be activated by transition metals to produce strong sulfate radicals, called Fenton-like reaction (i.e., R5) [69]. In this case, Fe ions (Fe^{2+}) dissolved in water from Fe_3O_4 and TF and those available in solid Fe_3O_4 and TF can activate PS. PS/TiO_2 also showed relatively high reactivity because a trace level of transition metals present in TiO_2 as impurities might have triggered a Fenton-like reaction. It was reported that even small amounts of transition metals, much less than 2 mg/L (as a threshold concentration), are effective to activate oxidants for the generation of radicals [68-70].

2-4. UV-LED/PS/Catalysts

Removal of IMD by the most complex combinational systems is shown in Fig. 6(d). UV-LED/PS (R3 and R4) was very effective. Compared with PS only (R3 shown in Fig. 6(c)), the high reactivity of UV-LED/PS could be explained by photolysis of PS to generate sulfate radicals ($SO_4^{\bullet-}$) for the fast oxidation of IMD, i.e., R4 mechanism. Interestingly, UV-LED/TiO_2/PS combining R3, R4, R6, and A1 (presumably R5 as well) and UV-LED/Fe_3O_4/PS combining R3, R4, R5, and A1 (presumably R6 as well) were slightly more effective than UV-LED/PS combining R3 and R4. Considering adsorption of IMD to TiO_2 and Fe_3O_4 (A1), contribution of R5 and R6 to IMD decomposition was not as significant as for persulfate. In addition, it is crystal clear that because of the more powerful oxidative nature of PS and relatively high concentration of that (in this test only), it acts much better than individual catalysts. Actually, there is no doubt that individual catalysts did not perform as good as oxidative or photo-oxidative procedure. Meanwhile, UV-LED/TF/PS combining R3, R4, R5, R6 and A1 showed the best reactivity to remove IMD. TF was consistently superior to TiO_2 and Fe_3O_4 in all cases combining it with any photochemical and photocatalytic processes. Only UV-LED/TF/PS achieved pseudo-stead state after 4 hr of reaction.

3. Parametric Studies for UV-LED/TF/PS

Parametric studies to evaluate the effects of PS concentration, IMD concentration, and circulation rate on IMD decomposition kinetics were performed for the best combinational system, UV-LED/TF/PS.

The effect of PS concentration on IMD decomposition kinetics in the absence of TF (i.e., R3+R4) and presence of TF (i.e., R3+R4+R5+R6+A1) is shown in Fig. 7. It was confirmed that the absence of both PS and TF (R1 and R2 mechanisms only) did not show decomposition of IMD. TF without PS (R6 and A1 mecha-

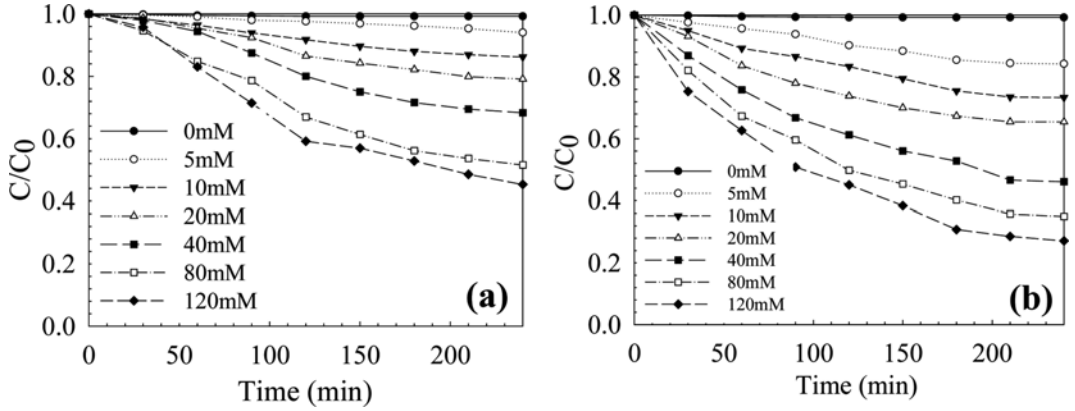

Fig. 7. Effect of PS concentration at 0-120 mM on IMD decomposition kinetics: (a) In the absence of TF and (b) in the presence of TF (UV-LED=66 W, I=1.40 A, $pH_{initial}$~6, T=25 °C, [TF]=250 mg/L, [IMD]=20 mg/L, and circulation rate=100 mL/min).

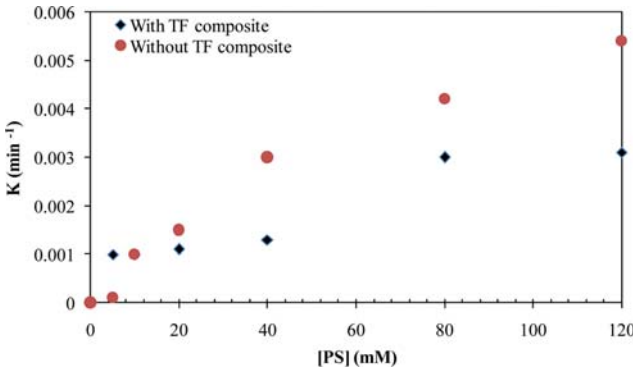

Fig. 8. Effect of PS concentration at 0-120 mM on IMD degradation rate constant, k: (a) In the absence of TF and (b) in the presence of TF (UV-LED=66 W, I=1.40 A, $pH_{initial}$~6, T=25 °C, [TF]=250 mg/L, [IMD]=20 mg/L, and circulation rate=100 mL/min).

nisms only) also showed no decomposition of IMD. As PS concentration increased, which affected R3, R4 and R5 mechanisms, IMD decomposed faster. Similar pattern was observed regardless of the presence of TF. The presence of TF slightly improved IMD removal due to the addition of R5, R6, and A1 mechanisms. However, as observed previously, the contribution of R5 and R6 was not significant, considering that IMD adsorption onto TF (A1) was also in place. R3 and R4 mechanisms already significantly contributed to IMD removal. IMD removal followed first-order kinetics and thus first-order reaction rate constants were summarized in Fig. 8. Increase in PS concentration resulted in higher reaction rates. Impact of PS was more significant in the presence of TF.

The effect of IMD concentration on its decomposition kinetics is shown in Figs. 9 and 10. IMD decomposition kinetics significantly decreased almost linearly over initial IMD concentration. There was competition for UV photon energy among direct photolysis of IMD (R2), photolysis of PS (R4), and photocatalysis (R6), which was influenced by initial IMD concentration. At higher IMD concentration, adsorption of IMD to TF (A1) might be more significant. Many factors alone and in combination might have been

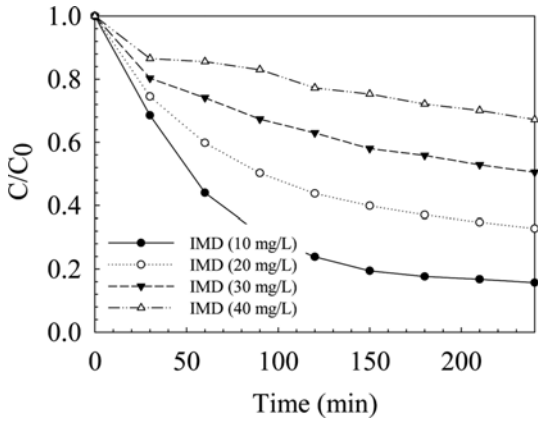

Fig. 9. Effect of IMD concentration on IMD decomposition kinetics (UV-LED=66 W, I=1.40 A, $pH_{initial}$~6, T=25 °C, [TF]=250 mg/L, [PS]=20 mM, and circulation rate=100 mL/min).

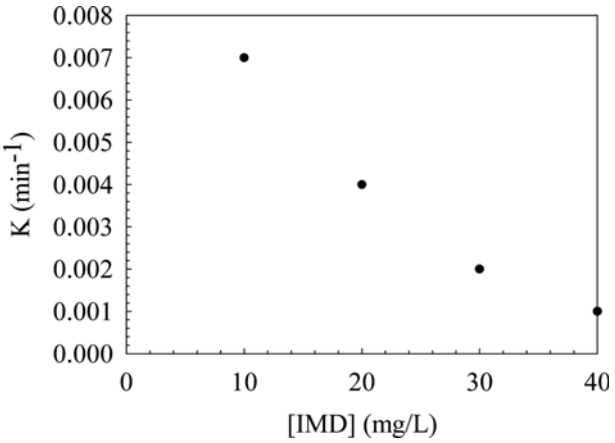

Fig. 10. Effect of IMD concentration on IMD degradation rate constant, k (UV-LED=66 W, I=1.40 A, $pH_{initial}$~6, T=25 °C, [TF]=250 mg/L, [PS]=20 mM, and circulation rate=100 mL/min).

involved in the observed results. Note that the y-axis is normalized concentration of IMD. The total amount of IMD removed over time

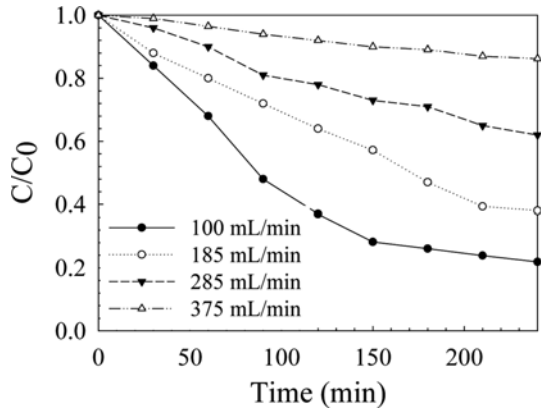

Fig. 11. Effect of circulation rate at 100-375 mL/min on IMD decomposition kinetics (UV-LED=66 W, I=1.40 A, $pH_{initial}$~6, T=25 °C, [TF]=250 mg/L, [IMD]=20 mg/L, and [PS]=20 mM).

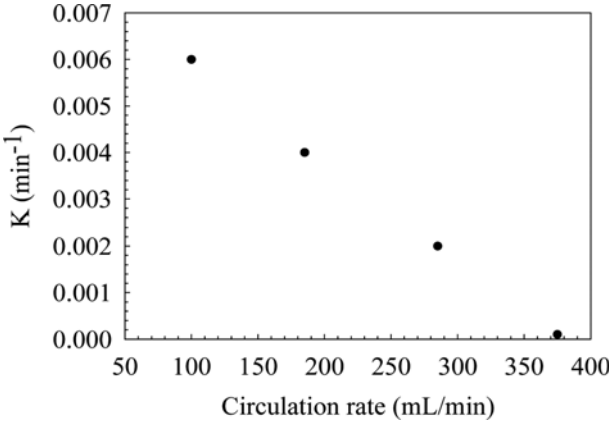

Fig. 12. Effect of circulation rate on IMD degradation rate constant, k (UV-LED=66 W, I=1.40 A, $pH_{initial}$~6, T=25 °C, [TF]=250 mg/L, [IMD]=20 mg/L, and [PS]=20 mM).

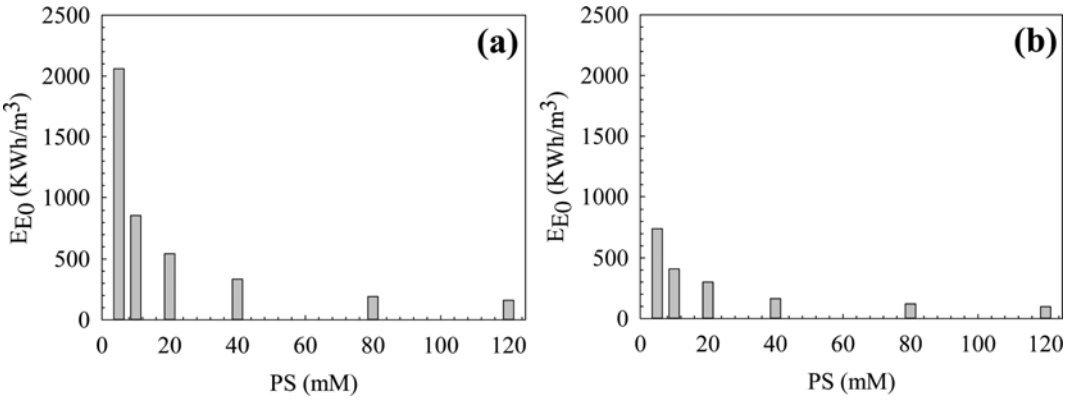

Fig. 13. Effect of PS concentration at 0-120 mM on electrical energy consumption during degradation of IMD (a) in absence of TF and (b) in the presence of TF (UV-LED=66 W, I=1.40 A, $pH_{initial}$~6, T=25 °C, [TF]=250 mg/L, [IMD]=20 mg/L, and circulation rate=100 mL/min).

was more or less similar regardless of initial IMD concentration.

The effect of internal circulation rate in UV-LED photoreactor on IMD decomposition kinetics is shown in Figs. 11 and 12. Increasing circulation rate from 100 mL/min to 375 mL/min greatly reduced IMD decomposition. Decomposition rate constants also almost linearly decreased over circulation rate. This result is interesting because the reactor is batch-type. IMD and PS were first introduced to the second chamber (2,500 mL) with TF under UV-LED irradiation, continuously moved to the first chamber (5,000 mL) under UV-LED irradiation without TF, and then circulated for 4 hr. All chemicals stayed in the first reactor for average 160 min and in the second reactor for average 80 min regardless of circulation, resulting in HRT or total reaction time of 4 hr. R3, R4, R5, R6 and A1 mechanisms occurred in the second chamber, while only R3 and R4 mechanisms occurred in the first chamber. Although circulation rate does not affect HRT in each chamber, circulation can speed up movement of chemicals between the chambers, i.e., chamber 2→chamber 1→chamber 2→chamber 1→… If there is no circulation, ⅓-rd of IMD molecules will stay only in the second chamber and ⅔-rds of them will stay only in the first chamber. If there is high circulation, all IMD molecules will stay in the second chamber shortly, then continuously move to/stay in the first chamber shortly and recirculate quickly. The difference might have impacted IMD decomposition kinetics somehow, which should be thoroughly investigated in a follow-up study.

4. Electrical Energy Consumption

In addition to IMD decomposition kinetics of the various UV-LED/PS/TF systems, their electrical energy consumption is an important factor which impacts their scale-up later and practical applications under solar radiation. The results on the effects of PS concentration, IMD concentration, and circulation rate (shown in Figs. 7, 9, and 11) were reconstructed to determine their effects on electrical energy consumption. Energy consumption was measured using Eq. (1) proposed by International Union of Pure and Applied Chemistry, where E_{E0} is electrical energy cost or consumption (KWh/m^3) and thus electrical energy efficiency, P is power of irradiation source (kW), t is time of irradiation (min), V is volume of water (L), and C_i and C_f are the initial and final concentrations of IMD (mg/L) [71]. In particular, $t/\log(C_i/C_f)$ in the equation represents the inverse of the first-order rate constant of the reaction.

$$E_{E0} = \frac{1000 \times P \times t}{60 \times V \times \log(C_i/C_f)} \quad (1)$$

The effect of PS concentration is shown in Fig. 13. Apparently, increase in PS dose significantly decreased electrical energy consumption. The presence of TF significantly reduced electrical energy consumption. The observation was more remarkable in the range of low PS concentrations because even a small amount of PS could significantly trigger R3, R4 and R5 mechanisms. As a result, use of TF than TiO_2 or Fe_3O_4 as well as introduction of PS was crucial to enhance reaction kinetics and thus to reduce energy consumption. Similarly to PS concentration, the effects of IMD concentration and circulation rate on electrical energy consumption are shown in Figs. 14 and 15, respectively. As expected from the previous results, increasing IMD concentration and circulation rate resulted in more energy consumption.

5. Reusability Assessment

Reusability of TF was briefly assessed for six cycles, as shown in Fig. 16. The experiment was conducted in UV-LED/TF/PS system under standard conditions. Once pseudo-steady state of IMD decomposition for 4 hr was achieved, the reaction solution in the

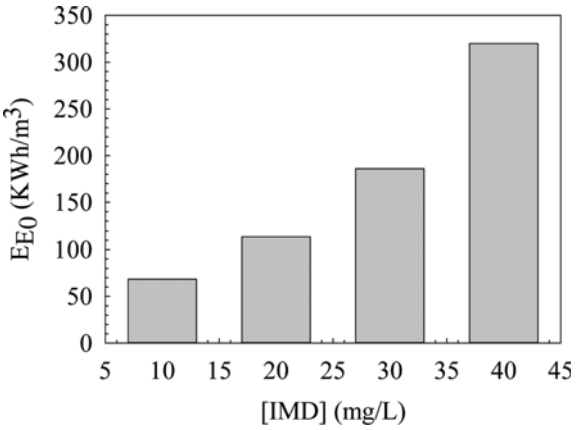

Fig. 14. Effect of IMD concentration at 10-40 mg/L on electrical energy consumption during degradation of IMD (UV-LED=66 W, I=1.40 A, $pH_{initial}$~6, T=25 °C, [TF]=250 mg/L, [PS]=20 mM, and circulation rate=100 mL/min).

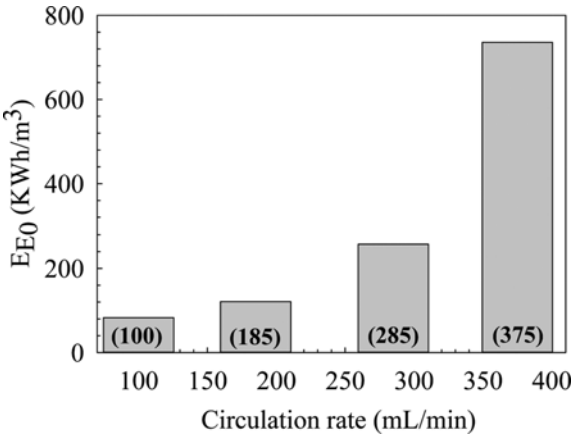

Fig. 15. Effect of circulation rate at 100-375 mL/min on electrical energy consumption during degradation of IMD (UV-LED= 66 W, I=1.40 A, $pH_{initial}$~6, T=25 °C, [TF]=250 mg/L, [IMD]= 20 mg/L, and [PS]=20 mM).

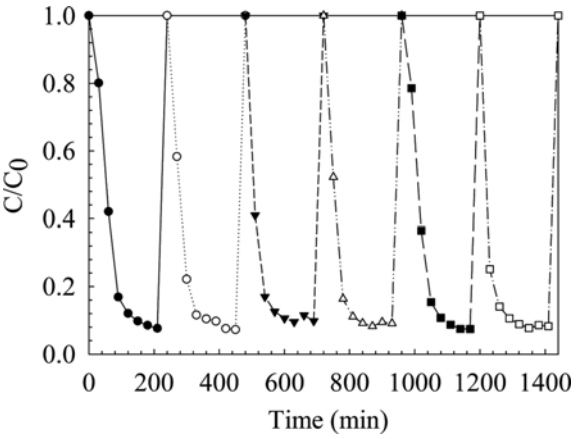

Fig. 16. Reactivity change of TF immobilized onto glass tubes upon repeated use (6 cycles) with respect to degradation of IMD (UV-LED=66 W, I=1.40 A, $pH_{initial}$~6, T=25 °C, [TF]=250 mg/L, [IMD]=20 mg/L, [PS]=20 mM, and circulation rate= 100 mL/min).

reactor was decanted and TF was dried under ambient condition. Then, the reactor was recharged with new IMD solution. For six cycles, almost the same decomposition pattern was observed. The result indicated that TF catalyst was firmly attached to the glass tubes and it was not deactivated over the cycles. Furthermore, spent solution after each cycle was analyzed using an atomic absorption spectrometer (*Varian 240AA*, *Agilent*, *Australia*) to detect any probable released or un-attached particles from the substrate of the utilized catalysts. Analysis did not show any important amounts for toxic heavy metals such as Fe or Ti in final solution.

CONCLUSIONS

TF nanocomposite combining photocatalytic TiO_2 and magnetic Fe_3O_4 was successfully synthesized and immobilized onto glass tubes to build a photocatalytic reactor for the removal of IMD. PS was injected to the reactor under irradiation with UV-LED powered by PV. Various control and reference tests and parametric studies enabled us to explain different IMD removal mechanisms including self-decomposition, direct photolytic decomposition, chemical oxidation by PS, photolysis of PS to produce sulfate radicals, Fenton-like reaction to produce sulfate radicals, photocatalysis to generate hydroxyl radicals, and adsorption onto catalysts. The reactivity increased in order of UV-LED<TiO_2<Fe_3O_4≈TF< UV-LED/Fe_3O_4≈UV-LED/TiO_2<UV-LED/TF<PS<<TiO_2/PS<Fe_3O_4/ PS<PS/TF<UV-LED/PS<<UV-LED/TiO_2/PS<UV-LED/Fe_3O_4/PS< UV-LED/TF/PS. TF conjugated with PS under UV-LED was able to most synergistically remove IMD by combining all the removal mechanisms. Use of TF than TiO_2 or Fe_3O_4 and introduction of even a small amount of PS significantly contributed to decreasing energy consumption. Consequences illustrated that the synergy index factor of 75%, 65%, and 60% for IMD removal was achieved by UV-LED/TF/PS, UV-LED/Fe_3O_4/PS, and UV-LED/TiO_2/PS routes, respectively. Since all devices used in this study were powered solely by a PV module, the photocatalytic reactor is proposed as a sustainable, self-powered, energy-saving, and practical point-of-use decontamination system to remove organic contaminants in water under UV-LED powered by solar radiation.

ACKNOWLEDGEMENTS

Dr. Eskandarian thanks the University of Zanjan and Semnan University for providing financial support for this work. Dr. Choi also acknowledges partial financial support for this research by the University of Texas at Arlington.

SUPPORTING INFORMATION

Additional information as noted in the text. This information is available via the Internet at http://www.springer.com/chemistry/journal/11814.

REFERENCES

1. M. A. Shannon, P. W. Bohn, M. Elimelech, J. G. Georgiadis, B. J. Mariñas and A. M. Mayes, *Nature*, **452**, 301 (2008).
2. M. A. Montgomery and M. Elimelech, *Environ. Sci. Technol.*, **41**, 17 (2007).
3. M. H. Rasoulifard, M. Akrami and M. R. Eskandarian, *J. Taiwan Inst. Chem. Eng.*, **57**, 77 (2015).
4. J.-L. Liu and M.-H. Wong, *Environ. Int.*, **59**, 208 (2013).
5. R. Loos, G. Locoro, S. Comero, S. Contini, D. Schwesig, F. Werres, P. Balsaa, O. Gans, S. Weiss and L. Blaha, *Water Res.*, **44**, 4115 (2010).
6. K. Fenner, S. Canonica, L. P. Wackett and M. Elsner, *Science*, **341**, 752 (2013).
7. Label Review Manual for Pesticides, U.S. Environmental Protection Agency, 2015, http://www.epa.gov/oppfead1/labeling/lrm/chap-07.
8. E. Mathioulakis, V. Belessiotis and E. Delyannis, *Desalination*, **203**, 346 (2007).
9. H. Choi, S. R. Al-Abed, D. D. Dionysiou, E. Stathatos and P. Lianos, *Sustain. Sci. Eng.*, **2**, 229 (2010).

10. A. R. Ribeiro, O. C. Nunes, M. F. R. Pereira and A. M. T. Silva, *Environ. Int.*, **75**, 33 (2015).
11. H. Park, H. Kim, G. Moon and W. Choi, *Energy Environ. Sci.*, **9**, 411 (2016).
12. A. Dhakshinamoorthy, S. Navalon, A. Corma and H. Garcia, *Energy Environ. Sci.*, **5**, 9217 (2012).
13. R. E. Galian and J. Perez-Prieto, *Energy Environ. Sci.*, **3**, 1488 (2010).
14. R. T. Koodali and D. Zhao, *Energy Environ. Sci.*, **3**, 608 (2010).
15. W.-W. Li, H.-Q. Yu and Z. He, *Energy Environ. Sci.*, **7**, 911 (2014).
16. S. J. A. Moniz, S. A. Shevlin, D. J. Martin, Z.-X. Guo and J. Tang, *Energy Environ. Sci.*, **8**, 731 (2015).
17. J. Zhang, Y. Wu, M. Xing, S. A. K. Leghari and S. Sajjad, *Energy Environ. Sci.*, **3**, 715 (2010).
18. T. Su, Q. Shao, Z. Qin, Z. Guo and Z. Wu, *Acs Catal.*, **8**, 2253 (2018).
19. R. Ma, L. Dong, B. Li, T. Su, X. Luo, Z. Qin and H. Ji, *ChemistrySelect.*, **3**, 5891 (2018).
20. O. Legrini, E. Oliveros and A. M. Braun, *Chem. Rev.*, **93**, 671 (1993).
21. J. Schneider, M. Matsuoka, M. Takeuchi, J. Zhang, Y. Horiuchi, M. Anpo and D. W. Bahnemann, *Chem. Rev.*, **114**, 9919 (2014).
22. E. Brillas, I. Sirés and M. A. Oturan, *Chem. Rev.*, **109**, 6570 (2009).
23. M. Pelaez, P. Falaras, A. G. Kontos, A. Armah, K. O'shea, P. S. M. Dunlop, J. A. Byrne and D. D. Dionysiou, *Appl. Catal. B Environ.*, **121**, 30 (2012).
24. J. Deng, Y. Shao, N. Gao, S. Xia, C. Tan, S. Zhou and X. Hu, *Chem. Eng. J.*, **222**, 150 (2013).
25. X. Van Doorslaer, K. Demeestere, P. M. Heynderickx, H. Van Langenhove and J. Dewulf, *Appl. Catal. B Environ.*, **101**, 540 (2011).
26. A. O. Kondrakov, A. N. Ignatev, F. H. Frimmel, S. Bräse, H. Horn and A. I. Revelsky, *Appl. Catal. B Environ.*, **160**, 106 (2014).
27. T. Alapi and A. Dombi, *J. Photochem. Photobiol. A Chem.*, **188**, 409 (2007).
28. R. F. Dantas, O. Rossiter, A. K. R. Teixeira, A. S. M. Simões and V. L. da Silva, *Chem. Eng. J.*, **158**, 143 (2010).
29. S. Sanches, M. T. B. Crespo and V. J. Pereira, *Water Res.*, **44**, 1809 (2010).
30. S. Bounty, R. A. Rodriguez and K. G. Linden, *Water Res.*, **46**, 6273 (2012).
31. C. Pablos, J. Marugán, R. van Grieken and E. Serrano, *Water Res.*, **47**, 1237 (2013).
32. A. Adak, K. P. Mangalgiri, J. Lee and L. Blaney, *Water Res.*, **70**, 74 (2015).
33. S. Chakma, S. Praneeth and V. S. Moholkar, *Ultrason. Sonochem.*, **38**, 652 (2017).
34. S. Chakma and V. S. Moholkar, *Indian Chem. Eng.*, **57**, 359 (2015).
35. M. M. Khin, A. S. Nair, V. J. Babu, R. Murugan and S. Ramakrishna, *Energy Environ. Sci.*, **5**, 8075 (2012).
36. M. Wang, J. Ioccozia, L. Sun, C. Lin and Z. Lin, *Energy Environ. Sci.*, **7**, 2182 (2014).
37. I. Ali, *Chem. Rev.*, **112**, 5073 (2012).
38. M. Rasoulifard, M. Fazli and M. Eskandarian, *J. Ind. Eng. Chem.*, **20**, 3695 (2014).
39. L. Tan, X. Zhang, Q. Liu, X. Jing, J. Liu, D. Song, S. Hu, L. Liu and J. Wang, *Colloids Surfaces A Physicochem. Eng. Asp.*, **469**, 279 (2015).
40. M. A. Habila, Z. A. ALOthman, A. M. El-Toni, J. P. Labis and M. Soylak, *Talanta*, **154**, 539 (2016).
41. T. Xin, M. Ma, H. Zhang, J. Gu, S. Wang, M. Liu and Q. Zhang, *Appl. Surf. Sci.*, **288**, 51 (2014).
42. J. Zhan, H. Zhang and G. Zhu, *Ceram. Int.*, **40**, 8547 (2014).
43. P. Zhang, Z. Mo, L. Han, X. Zhu, B. Wang and C. Zhang, *Ind. Eng. Chem. Res.*, **53**, 8057 (2014).
44. Q. He, Z. Zhang, J. Xiong, Y. Xiong and H. Xiao, *Opt. Mater. (Amst)*, **31**, 380 (2008).
45. T. Harifi and M. Montazer, *Sep. Purif. Technol.*, **134**, 210 (2014).
46. F. Deng, Y. Li, X. Luo, L. Yang and X. Tu, *Colloids Surfaces A Physicochem. Eng. Asp.*, **395**, 183 (2012).
47. S. Vilhunen and M. Sillanpää, *Rev. Environ. Sci. Bio/Technology*, **9**, 323 (2010).
48. W. Jo, G. T. Park and R. J. Tayade, *J. Chem. Technol. Biotechnol.*, **90**, 2280 (2015).
49. E. Korovin, D. Selishchev, A. Besov and D. Kozlov, *Appl. Catal. B Environ.*, **163**, 143 (2015).
50. Q. Zhang, C.-F. Wang, L.-T. Ling and S. Chen, *J. Mater. Chem. C*, **2**, 4358 (2014).
51. M. R. Eskandarian, M. Fazli, M. H. Rasoulifard and H. Choi, *Appl. Catal. B Environ.*, **183**, 407 (2016), DOI:10.1016/j.apcatb.2015.11.004.
52. M. R. Eskandarian, H. Choi, M. Fazli and M. H. Rasoulifard, *Chem. Eng. J.*, **300**, 414 (2016), DOI:10.1016/j.cej.2016.05.049.
53. M. D. Sobsey, Managing water in the home: accelerated health gains from improved water supply, World Health Organization (2002).
54. S. Gundry, M. Sobsey and J. Wright, *Waterlines.*, **23**, 14 (2005).
55. J. Brown and M. D. Sobsey, *Am. J. Trop. Med. Hyg.*, **87**, 394 (2012).
56. D. Mäusezahl, A. Christen, G. D. Pacheco, F. A. Tellez, M. Iriarte, M. E. Zapata, M. Cevallos, J. Hattendorf, M. D. Cattaneo and B. Arnold, *PLoS Med.*, **6**, e1000125 (2009).
57. B. Parida, S. Iniyan and R. Goic, *Renew. Sustain. Energy Rev.*, **15**, 1625 (2011).
58. O. Autin, C. Romelot, L. Rust, J. Hart, P. Jarvis, J. MacAdam, S. A. Parsons and B. Jefferson, *Chemosphere*, **92**, 745 (2013).
59. M. A. Würtele, T. Kolbe, M. Lipsz, A. Külberg, M. Weyers, M. Kneissl and M. Jekel, *Water Res.*, **45**, 1481 (2011).
60. M. A. S. Ibrahim, J. MacAdam, O. Autin and B. Jefferson, *Environ. Technol.*, **35**, 400 (2014).
61. C. Chatterley and K. Linden, *J. Water Health*, **8**, 479 (2010).
62. G. Y. Lui, D. Roser, R. Corkish, N. Ashbolt, P. Jagals and R. Stuetz, *Sci. Total Environ.*, **493**, 185 (2014).
63. G. Y. Lui, D. Roser, R. Corkish, N. J. Ashbolt and R. Stuetz, *Sci. Total Environ.*, **553**, 626 (2016).
64. O. Iglesias, J. Gómez, M. Pazos and M. Á. Sanromán, *Appl. Catal. B Environ.*, **144**, 416 (2014).
65. S. Wu, A. Sun, F. Zhai, J. Wang, W. Xu, Q. Zhang and A. A. Volinsky, *Mater. Lett.*, **65**, 1882 (2011).
66. Y. Eom, M. Abbas, H. Noh and C. Kim, *RSC Adv.*, **6**, 15861 (2016).
67. S. Liu, K. Yao, L.-H. Fu and M.-G. Ma, *RSC Adv.*, **6**, 2135 (2016).
68. G. P. Anipsitakis and D. D. Dionysiou, *Environ. Sci. Technol.*, **37**, 4790 (2003).
69. G. P. Anipsitakis and D. D. Dionysiou, *Environ. Sci. Technol.*, **38**, 3705 (2004).
70. Z. Xu, C. Shan, B. Xie, Y. Liu and B. Pan, *Appl. Catal. B Environ.*, **200**, 439 (2017).
71. J. R. Bolton, K. G. Bircher, W. Tumas and C. A. Tolman, *Pure Appl. Chem.*, **73**, 627 (2001).

Supporting Information

Synergistic decomposition of imidacloprid by TiO_2-Fe_3O_4 nanocomposite conjugated with persulfate in a photovoltaic-powered UV-LED photoreactor

Mohammad Reza Eskandarian[*,,***], Mohammad Hossein Rasoulifard[**,†], Mostafa Fazli[*], Leila Ghalamchi[**], and Hyeok Choi[***,†]**

*Department of Applied Chemistry, Faculty of Chemistry, Semnan University, Semnan 363-35196, Iran
**Water & Wastewater Treatment Research Laboratory, Department of Chemistry, University of Zanjan, Zanjan 313-45195, Iran
***Department of Civil Engineering, The University of Texas at Arlington, Arlington, TX 76019-0308, United States
(*Received 9 October 2018 • accepted 17 January 2019*)

Table S1 Chemical properties of imidacloprid [6,7]

Name	Imidacloprid (IMD)
Chemical name (IUPAC)	N-{1-[(6-Chloro-3-pyridyl)methyl]-4,5-dihydroimidazol-2-yl}nitramide
Category	Insecticide
Type	Imidazole
CAS number	138261-41-3
Molecular mass (g/L)	255.661
Chemical formula	$C_9H_{10}ClN_5O_2$
Appearance	Colorless crystals
Water solubility	0.51 g/L at 20 °C
Molecular structure	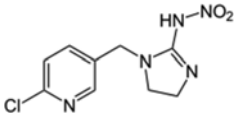

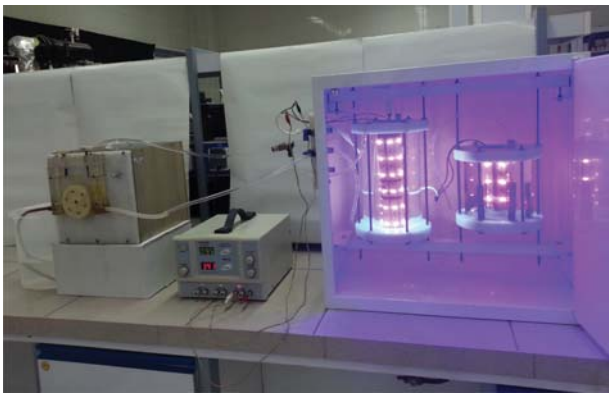

Fig. S1. Photovoltaics-powered UV-LED photoreactor with various accessories including power controller, pristalitic pump, and glass tubes coated with TF composite. All devices used in this study are powered by a photovoltaic module.

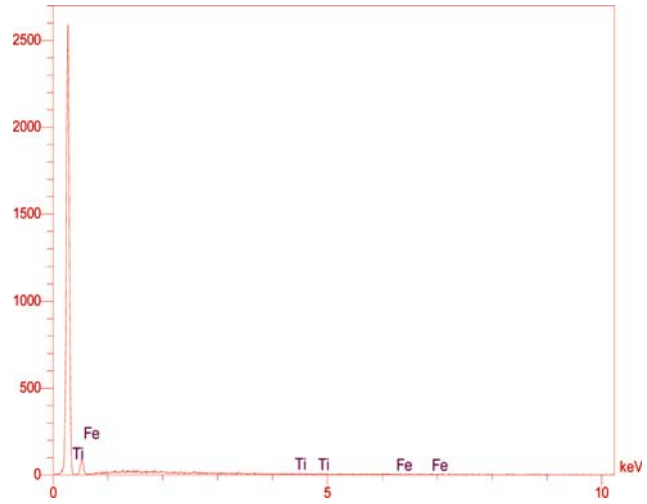

Fig. S2. EDX of TF composite.

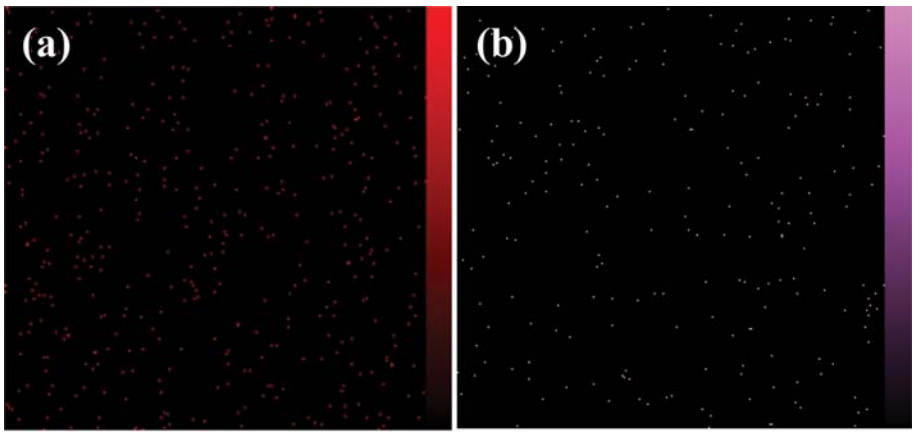

Fig. S3. Elemental mapping of TF composite coated onto glass surface: (a) Ti distribution and (b) Fe distribution.

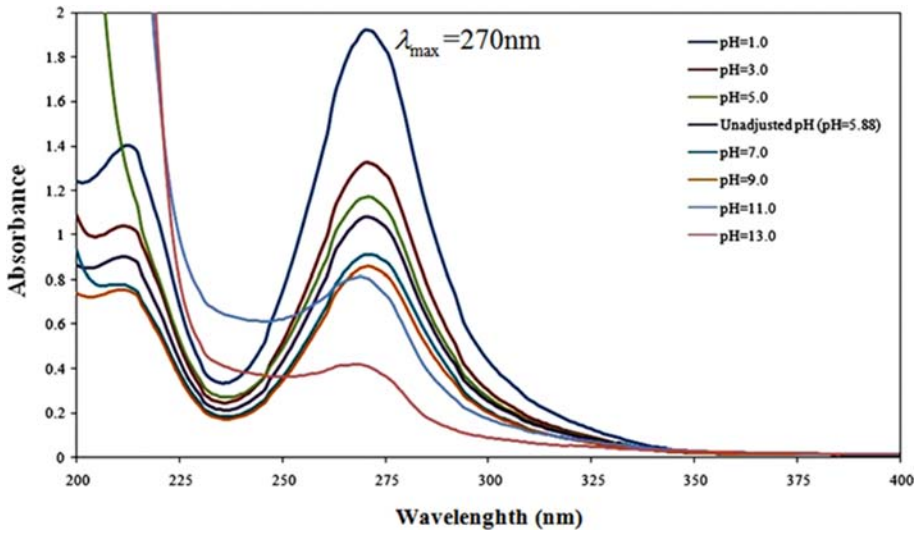

Fig. S4. UV-vis spectra for IMD at different pH (λ_{max}=270 nm).